THE JOURNAL OF PHYSICAL CHEMISTRY Letters

Letter

pubs.acs.org/JPCL

Pushing the Sample-Size Limit of Infrared Vibrational Nanospectroscopy: From Monolayer toward Single Molecule Sensitivity

Xiaoji G. Xu,[†] Mathias Rang,[‡] Ian M. Craig,[§] and Markus B. Raschke*[,†]

[†]Department of Physics, Department of Chemistry, and JILA, University of Colorado, Boulder, Colorado 80309, United States

[‡]Forschungsinstitut am Goetheanum, CH-4143 Dornach, Switzerland

[§]Pacific Northwest National Laboratory, Richland, Washington 99352, United States

Supporting Information

ABSTRACT: While scattering-scanning near-field optical microscopy (*s*-SNOM) has demonstrated its potential to extend infrared (IR) spectroscopy into the nanometer scale, it has not yet reached its full potential in terms of spectroscopic sensitivity. We combine broadband femtosecond mid-IR excitation with an optimized spectral irradiance of ~2 W/cm^2/ cm^{-1} (power/area/bandwidth) and a combination of tip- and substrate enhancement to demonstrate single-monolayer sensitivity with exceptional signal-to-noise ratio. Using interferometric time domain detection, the near-field IR *s*-SNOM spectral phase directly reflects the molecular vibrational resonances and their intrinsic line shapes. We probe the stretching resonance of ~1000 carbonyl groups at 1700 cm^{-1} in a self-assembled monolayer of 16-mercaptohexadecanoic acid (MHDA) on an evaporated gold substrate with spectroscopic contrast and sensitivity of $\lesssim$100 vibrational oscillators. From these results we provide a roadmap for achieving true single-molecule IR vibrational spectroscopy in *s*-SNOM by implementing optical antenna resonant enhancement, increased spectral pump power, and improved detection schemes.

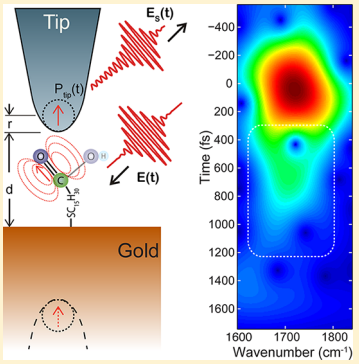

SECTION: Physical Processes in Nanomaterials and Nanostructures

Vibrational spectroscopy in its many forms provides a wealth of information on molecular systems. Among others, frequency resolution provides chemical identification, and symmetry selection rules allow measurement of relative bond orientation. It thus contributes to our understanding of material composition, molecular organization, intra- and intermolecular coupling, and chemical kinetics and dynamics.

Extension into the nanoscale for simultaneous ultrahigh spatial resolution has been enabled by the complementary optical techniques of tip-enhanced Raman spectroscopy (TERS)[1] and infrared vibrational scattering-scanning near-field optical microscopy (IR *s*-SNOM).[2] Additionally, for certain robust samples, single molecule[3] and even intramolecular[4] spatially resolved vibrational spectra have been measured by inelastic electron tunneling spectroscopy. However, the latter approach requires ultrahigh vacuum, conducting samples, and cryogenic temperatures.

Pushing sensitivity, contrast, spectral information, and spatial resolution of IR spectroscopy and microscopy has been a long-standing desire and challenge in general.[5−7] Subwavelength resolution vibrational IR spectroscopy would be particularly beneficial for investigations of soft organic matter, such as polymers, biomolecules, liquid crystals, self-assembled monolayers (SAMs), and molecular nanocomposites. There are few techniques other than IR *s*-SNOM that could provide nanoscale identification and mapping of these materials, especially under ambient conditions, and many important vibrational modes are either weak in Raman scattering, or by selections rules only allowed in IR spectroscopy.

While TERS has reached the monolayer and single molecule limit,[1,8,9] despite orders of magnitude larger vibrational IR cross sections ($\sigma_{abs}^{IR} \sim 10^{-18}$ cm^2/molecule for IR vs $\sigma_{scat}^{Raman} \sim 10^{-31}$ cm^2/molecule/sr for Raman), the spectroscopic sensitivity of IR *s*-SNOM has been limited to molecular sample volumes on the order of tens of nanometers in size[10−15] in part due to low IR detection sensitivity, the presence of interfering background signals, and the lack of optimal IR sources.[16] The general challenge in extending the range of molecular spectroscopy techniques to the ultimate single molecule sensitivity limit is intimately linked to the combination of optical signal strength, detection sensitivity, contrast of signal to background, and spectral specificity of the molecular mode to be probed—parameters not a priori favorably fulfilled in IR *s*-SNOM.

As a linear elastic light scattering technique, the resonant molecular *s*-SNOM near-field signal needs to be discriminated against generally large far-field and nonresonant near-field background signal contributions. Despite several well developed modulation and interferometric techniques, the near-field

Received: April 17, 2012
Accepted: June 18, 2012
Published: June 18, 2012

discrimination that can be obtained is imperfect both in narrow band[17] and broad band *s*-SNOM[14] implementations. While monochromatic continuous wave lasers can provide a high spectral irradiance, they typically have limited tuning range, cannot readily be multiplexed, and spectral normalization can be difficult due to mode hopping and beam drift. On the other hand, the sensitivity in experiments using broadband laser[15] and thermal sources[18] has been limited by the available spectral irradiance.

In addition, just like for any experimental configurations that involve reflection and diffuse scattering,[19] the spectral *s*-SNOM response is affected by the coherent superposition of both the desired intrinsic material dielectric function with both resonant absorption and dispersion, and extrinsic nonresonant terms from tip size and geometry effects.[20,21] The complications that arise from the resulting nontrivial near-field polarization and the coherent coupling of multiple tip−sample scattering source terms result in complex dispersive line shapes that correlate with intrinsic vibrational energy and line shape, but not in a straightforward manner,[22,23] making the a priori mode assignment and spectral shape interpretation difficult.

Here we pursue a systematic approach to increase spectroscopic sensitivity in IR vibrational *s*-SNOM. The first step to accomplish this goal is to maximize both resonant near-field signal intensity and its contrast against the predominantly nonresonant near-field background by the appropriate choice of IR laser source. In choosing the IR source, one important figure of merit is the *spectral irradiance*, i.e., the infrared power delivered to the focus area in a given frequency range (power/area/bandwidth, or spectral power/area). By selecting excitation bandwidth of 80−100 cm^{-1} (fwhm) to exceed the vibrational line width of the molecular resonance of typically 20−50 cm^{-1} (fwhm) by no more than a factor of 2−5, most of the light is resonant with the vibrational mode of interest, thus already reducing contributions to interfering nonresonant processes.

Furthermore, using nearly transform limited pulses with ∼220 fs duration, the resonant near-field free-induction decay (FID) signal with dephasing times ranging from ∼300 fs to at most several ps can then be separated from the instantaneous nonresonant both near- and far-field background by interferometric time-domain *s*-SNOM signal measurement.[24] Lastly, the combination of broadband femtosecond mid-IR excitation with the interferometric heterodyne detection allows for a generalization and extension of the phase-contrast approach[22,25] from frequency to time domain. We show experimentally and theoretically that for molecular resonances over a wide parameter range, the near-field spectral phase directly reflects the vibrational energy and intrinsic line width. This provides for a compellingly simple way for the direct comparison of IR vibrational *s*-SNOM spectra with molecular far-field IR absorption spectra.

By combining the phase contrast approach with the improved signal-to-noise ratio (s/n) arising from our high spectral irradiance IR pump excitation together with both tip and substrate enhancement,[26] we are able to image a SAM of 16-mercaptohexadecanoic-acid (MHDA) on a gold surface with 25 nm spatial resolution and identify its carbonyl stretch vibrational energy and line width. Demonstrating an IR *s*-SNOM spectral sensitivity and contrast of ∼100 molecular oscillators, we are reaching for the first time into the realm of single-molecule IR spectroscopy.

Experimental Details. For the experiment, we constructed a broad-band femtosecond mid-IR *s*-SNOM spectrometer as shown in Figure 1a. Wavelength tunable (central wavelength

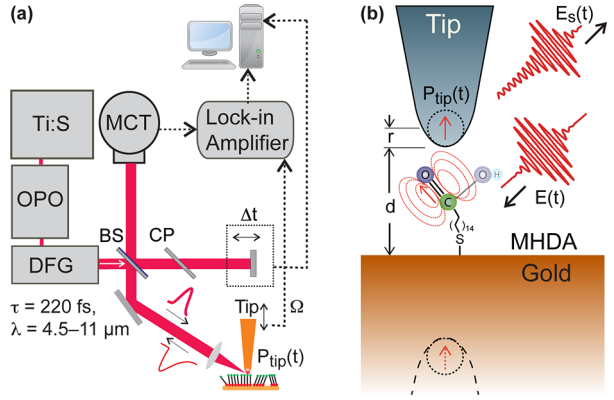

Figure 1. (a) Experimental setup of femtosecond IR *s*-SNOM. 220 fs broadband mid-IR pulses are generated by DFG of signal and idler output from an OPO. A 50:50 beamsplitter directs the beam into two arms of a Michelson interferometer, with the reference arm containing an additional uncoated compensation plate (CP) to balance the dispersion. The signal is focused onto a liquid nitrogen-cooled photoconductive MCT detector and digitized with a lock-in amplifier demodulated at the AFM tip drive frequency Ω and its harmonics. (b) A close-up view of the near-field tip−surface interaction. The incoming electric field $E(t)$ induces a polarization P_{tip} in the tip apex. The enhanced near-field electric field couples to the molecular carbonyl vibrational resonance in the MHDA monolayer, which modifies the scattered electric field $E_s(t)$.

∼4.5−11 μm) femtosecond mid-IR radiation at ∼1 mW average power, with pulse duration of ∼220 fs is generated by difference-frequency generation (DFG) of signal and idler from an optical parametric oscillator (OPO, Chameleon, APE) in a GeSe crystal.[27] The OPO is pumped by a Ti:Sapphire mode-locked oscillator with a pulse repetition rate of 76 MHz and an average power of 3.2 W at 800 nm (MiraHP, Coherent). After passing through a 50:50 IR beamsplitter (BS) in an asymmetric Michelson interferometer geometry, one-half of the light is focused (Ø ≃ 20 μm) onto the tip apex of a modified sample-scanning atomic force microscope (AFM, Innova, Bruker) with a gold coated off-axis parabolic reflector. A compensator plate (CP) in the reference arm assures equal dispersion. With 80 cm^{-1} spectral IR bandwidth we achieve a spectral irradiance of 2 $W/cm^2/cm^{-1}$, to our knowledge the highest of any broadband femtosecond IR *s*-SNOM experiment to date and key for achieving high sensitivity, yet below any noticeable sample degradation (see supplement for a table of irradiance from different mid-IR sources). The AFM operates in dynamic force mode with platinum coated tips (Arrow, NCPT, Nanosensors) driven at Ω ≃ 254 kHz and with a controlled peak-to-peak amplitude of 25 nm. The tip-scattered radiation is detected interferometrically by heterodyne amplification by a liquid nitrogen cooled mercury cadmium telluride (MCT) detector (J15D12-M204, Judson) with a high bandwidth transimpedance preamplifier (HVA-S, FEMTO). The near-field contribution is selected by lock-in demodulation (HF2Li, Zurich Instrument, 200 ms time constant) at harmonics of the tip oscillation frequency (Ω, 2Ω, and 3Ω). The pump light is polarized parallel to the tip axis for effective excitation of both the tip-dipole and the predominantly surface normal oriented

dx.doi.org/10.1021/jz300463d | *J. Phys. Chem. Lett.* 2012, 3, 1836−1841

carbonyl vibrational transition dipole for maximum near-field coupling (Figure 1b).

MHDA SAMs are prepared by immersing evaporated gold coated silicon wafers in a 1% solution of MHDA in ethanol for 24−48 h. For the measurements, the SAMs were removed from solution and blown dry without rinsing. The resulting MHDA SAM has a height of 2 nm and molecular density of ∼2 molecules/nm^2.[28] Cyclic dimerization and/or hydrogen bonding between neighboring MHDA molecules gives rise to a dominant carbonyl mode at 1699 cm^{-1}.[29,30]

Results. Figure 2 shows a simultaneously recorded topography (a) and IR *s*-SNOM image (b) acquired by spectrally

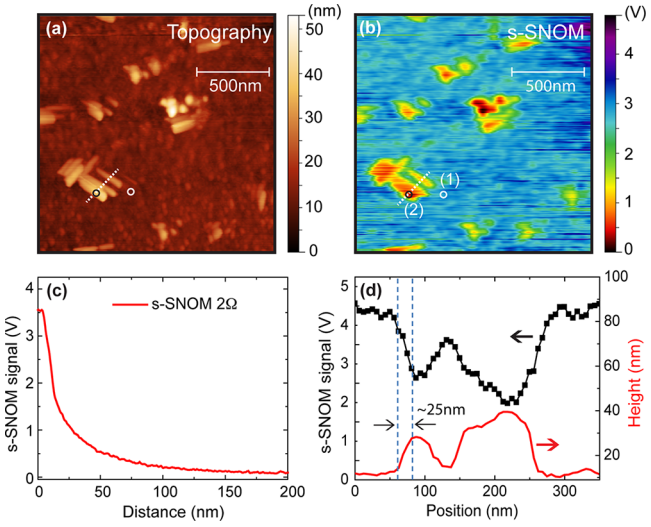

Figure 2. (a) Topography and (b) corresponding IR *s*-SNOM image collected simultaneously at 1700 cm^{-1} of an MHDA SAM on gold with MHDA nanocrystals. (c) Approach curve at second-harmonic (2Ω) demodulation on SAM showing a surface normal near-field localization of <25 nm. This, together with the *s*-SNOM line trace across the nanocrystals (d, along white dashed line in paneld a and b) indicates a spatial in- and out-of-plane resolution of ∼25 nm determined by the tip apex radius.

integrated detection without interferometric heterodyne amplification. The topography shows MHDA nanocrystals on top of the SAM formed after solvent evaporation from the excess MHDA. The fine structural variations on the SAM are due to the surface roughness of the underlying evaporated gold substrate. The *s*-SNOM image (b) is acquired at the second-harmonic (2Ω) demodulation without interferometric amplification with the laser tuned to the carbonyl resonance near ∼1700 cm^{-1}. The image contrast is not resonance specific in this case, because the spectrally integrated *s*-SNOM signal is dominated by the gold substrate enhancement.

Corresponding IR *s*-SNOM approach curves on the SAM region are shown in Figure 2c. This together with the signal line trace across a nanocrystal in Figure 2d demonstrates the near-field signature with ∼25 nm spatial resolution limited by the tip apex radius.[31] With the tip on top of a nanocrystal, despite the increase in number of molecules probed, a decrease in *s*-SNOM signal is observed as a result of the decrease in tip−sample coupling and metal−substrate enhancement with distance.

In order to obtain local vibrational spectroscopic information of the SAM, we performed interferometric heterodyne detection of the tip-scattered near-field signal (3Ω lock-in demodulation) as shown in Figure 3a (red, sample location (1) in Figure 2b), compared to the laser reference (black) consisting of scattering from the tip oscillating in free space. The high spectral irradiance of our DFG gives us good enough signal-to-noise, even in the higher demodulation harmonics, that we require no postprocessing smoothing or averaging beyond the 200 ms time constant of the lock-in.

The carbonyl resonant response from the SAM exhibits a characteristic resonant FID tail within ∼800 fs time delay. The resonant behavior is furthermore evident from the delayed signal rise at early negative time delay as expected and indicated by the arrows at the peak of the laser and *s*-SNOM spectrum. The strong peak near zero time delay is due to the instantaneous response from the nonresonant signal, and is especially pronounced due to the strong tip−sample coupling with the gold surface. Figure 2b highlights the region dominated by the carbonyl FID with destructive interference with the nonresonant response (highlighted by blue region). The prolonged signal modulations in both the reference and SAM traces is a result of the IR absorption in air from water overtone absorption in that spectral region. With its equal contribution to both interferometer arms, the signature is symmetric around zero time delay which allows for its discrimination. The water signal extends for several tens of picoseconds due to the spectrally narrow rovibrational gas phase response. Control experiments have been carried out under the same experimental conditions but with the laser tuned off resonance, and on bare gold surfaces instead of SAMs. In each case, no FID is observed, due to the absence of a surface resonant interaction (see Supporting Information).

To better visualize the content of the asymmetric interferograms, we use a short-time Fourier transform (STFT)[32] with a Gaussian time window function of width 200 fs to construct time-frequency spectrograms. As shown in Figure 3c,d for the SAM near-field signal and driving laser pulse, respectively, the spectro-temporal evolution highlights the carbonyl oscillator related phase behavior during the FID (white dashed box in Figure 3c) and the associated delayed signal maximum (white horizontal lines). Destructive interference features originating from the water bands (marked by two dashed white circles in Figure 3d) are symmetric with respect to zero time delay as indicated by the dashed horizontal line; whereas such features in Figure 3c become asymmetric due to the interference with the near-field carbonyl FID.

The scattered *s*-SNOM FID field is a convolution of the intrinsic tip/sample polarizability $\alpha_{\mathrm{eff}}(t)$ with the laser field $E(t)$, given by $\alpha_{\mathrm{eff}}(t)\otimes E(t)$ in the time domain. Similar to the case of the determination of the ultrafast plasmon dynamics,[33] we divide the Fourier transforms of the near-field FID interferogram with that of the laser for their deconvolution. The interferogram of the laser is an *autocorrelation* measurement of the laser field $E(t)$ in the time domain, therefore its Fourier transform provides the intensity spectrum of the laser field $E(\omega)E^*(\omega)$ as a purely real value. The interferogram of the near-field FID, however, is the *cross-correlation* between the laser field $E(t)$ and the scattered near-field $\alpha_{\mathrm{eff}}(t)\otimes E(t)$. The corresponding Fourier transform of the near-field FID then gives the complex valued $\alpha_{\mathrm{eff}}(\omega)E(\omega)E^*(\omega)$, with terms for amplitude and phase. By dividing the FID and laser Fourier transforms, $\alpha_{\mathrm{eff}}(\omega)$ can be obtained, with both amplitude $|\alpha_{\mathrm{eff}}(\omega)|$ and spectral phase $\theta(\alpha_{\mathrm{eff}}(\omega))$.

By applying that procedure to the data from Figure 3, one obtains the laser (black) and IR *s*-SNOM intensity (red) as seen in Figure 4a. The resulting normalized resonant *s*-SNOM

dx.doi.org/10.1021/jz300463d | *J. Phys. Chem. Lett.* 2012, 3, 1836−1841

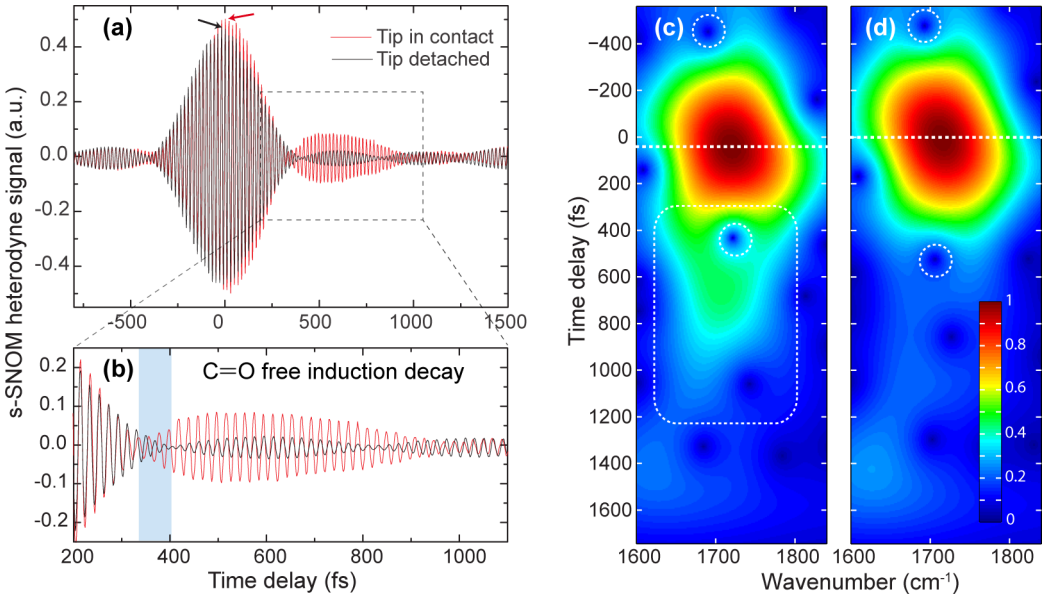

Figure 3. (a) SAM (red) and reference (black) *s*-SNOM interferograms with the carbonyl signature (asymmetric features, within initial 800 fs), strong nonresonant substrate-enhanced response at zero time delay, and long-lived modulation due to water overtone absorption (in both laser and *s*-SNOM signal). (b) Expansion of FID region showing the coherent evolution of the carbonyl FID with destructive interference (blue region). Corresponding STFT spectrograms of (c) SAM and (d) reference response highlights the distinct carbonyl FID tail.

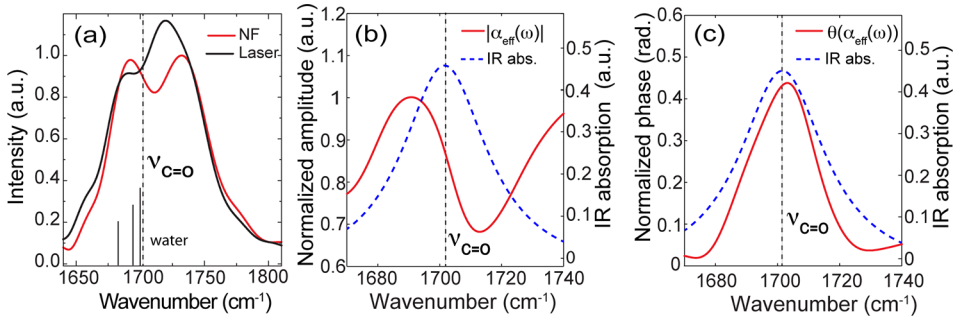

Figure 4. (a) Fourier transform of *s*-SNOM interferogram of SAM (red curve) and laser spectrum (black curve). Absorption dip in laser spectrum is due to the atmospheric water overtone absorption shown. (b) Normalized *s*-SNOM spectral amplitude of SAM near-field polarizability $|\alpha_{eff}(\omega)|$ shows dispersive line-shape. (c) Normalized spectral *s*-SNOM phase $\theta(\alpha_{eff}(\omega))$ resembles the infrared IR absorption profile (blue dashed line[29]) and allows for direct vibrational mode assignment.

spectral amplitude for the polarizability $|\alpha_{eff}(\omega)|$ and spectral phase $\theta(\alpha_{eff}(\omega))$ are shown in Figure 4b,c, respectively. The spectral amplitude and phase is independent of laser profile within the laser bandwidth. The spectrally unresolved water overtone lines at 1684, 1695, and 1700 cm^{-1} (spectral positions indicated in Figure 4a) are responsible for the dip in the laser spectrum but do not affect the normalized results (Figure 4b–c) as expected. This highlights one key advantage of the spectral phase approach demonstrated here in that the spectral near-field *s*-SNOM phase variation is largely insensitive to trace atmospheric gas absorption in the incident laser beam. Even without normalization, the absorption in air affects both signal and reference beam equally, and thus contributes only to the symmetric part of the interferogram and leads to an only negligible spectral phase variation (see Supporting Information).

The near-field intensity spectra (Figure 4b) exhibit a highly dispersive profile. As a coherent response, the *s*-SNOM signal is sensitive to both amplitude and phase of the combined resonant and nonresonant tip–sample interactions. The resulting interference is responsible for asymmetric spectral lineshapes. In traditional coherent spectroscopy, such dispersive spectral profiles can readily be analyzed by parametrized fitting. In *s*-SNOM, however, the spectral response obtained is also sensitive to extrinsic factors of geometry and resonances of the tip or, more generally, the dimensionality of the tip–sample coupling and phase effects in scattering (Mie scattering)—parameters difficult to know a priori. Yet, conceptually similar to coherent nonlinear vibrational spectroscopy,[34] and as has been observed before for the case of *s*-SNOM,[22,25] the spectral *s*-SNOM phase is expected to reflect the infrared absorption spectrum and allows for direct mode assignment. This behavior is seen in Figure 4c, where the spectral phase of the *s*-SNOM spectrum closely follows the far-field infrared vibrational absorption trace of the SAM, with the resonance from literature indicated by the dashed blue line.[29] The underlying mechanism is the weak spectral index of refraction change associated with molecular resonances.[12,19] Using the quasi-static image dipole model to describe the optical interaction between the tip and sample, we provide a phenomenological derivation of the effect (see Supporting Information for details). We show analytically that the spectral phase of the total effective polarizability α_{eff}

dx.doi.org/10.1021/jz300463d | J. Phys. Chem. Lett. 2012, 3, 1836–1841

responsible for the near-field scattering can be approximated by $\theta(\alpha_{eff}) = \theta(\alpha_{eff})_N + \theta(\alpha_{eff})_R \simeq \theta(\alpha_{eff})_N + f(d,\varepsilon_1,\alpha_1)\varepsilon_2(\omega)$. Here $\theta(\alpha_{eff})$ describes the effective phase of all nonresonant, $\theta(\alpha_{eff})_N$, and resonant, $\theta(\alpha_{eff})_R$, signal contributions in the frequency range of interest. $f(d,\varepsilon_1,\alpha_1)$ is a function dependent on the tip sample distance d, the real part of the resonant dielectric function ε_1, and the real part of the inverse of tip polarizability α_1. With ε_1 only weakly frequency dependent for typical vibrational resonances, i.e., weak dispersion, and $\varepsilon_2 = 2nk(\omega)$ for the molecular resonance, the spectral phase behavior is linearly proportional to the molecular extinction coefficient, and thus closely resembles the corresponding infrared absorption profile.

The slight shift in frequency between our spectral phase and the literature far-field spectrum seen in Figure 4c we attribute to the fact that the tip probes a nanoscale ensemble less inhomogeneously broadened than the macroscopic sample average. This is corroborated by the observation that the *s*-SNOM response is spectrally more narrow than the inhomogeneously broadened ensemble spectrum[24] The minor spectral differences observed in the near-field spectra between the SAM surface and the nanocrystal, taken at positions 1 and 2 in Figure 2, respectively, indicates cyclic dimer formation in both cases (see Supporting Information).

With our IR *s*-SNOM signal originating from a single molecular monolayer, our results demonstrate unprecedented spectroscopic sensitivity in IR *s*-SNOM. Assuming an ideal packing density for MHDA of 2 molecules/nm^2, and a near-field sampling area of $\sim(25\text{ nm})^2\ \pi/4 \simeq 500\text{ nm}^2$, we obtain a spectroscopic response from no more than 1000 molecules. This corresponds to a significant increase in sensitivity compared to even the best previous IR *s*-SNOM imaging and spectroscopy results,[10−13] and we achieve this sensitivity with a single interferogram without laser tuning, or data averaging. Judging from our s/n ratio of >10, we expect that as few as 100 molecules or molecular oscillators would suffice to generate a spectral phase response with identifiable vibrational energy under our current experimental conditions. Indeed, single proteins or other macromolecules can contain 100 or more oscillators, so this sensitivity already technically qualifies as a single molecule.

We expect that the sensitivity can readily be increased further. Simple measures such as dry nitrogen purging, maximal reflectance for all optical components, and optimized spectral sensitivity of the MCT detectors could already have provided an improvement by a factor of >2. Higher spectral irradiance could readily be achieved by higher power OPOs, more efficient DFG, or single step mid-IR OPOs.[35] This could deliver 10−50 mW with similar bandwidth and pulse duration, compared to our 1 mW IR power. Furthermore, replacing the commercial Pt-coated AFM tips conventionally used for *s*-SNOM with tips with engineered optical antenna resonances designed to match the molecular frequency range of interest would selectively enhance the resonant coupling between tips and molecular oscillators, improving signal intensity and contrast above the nonresonant background. Similarly, resonant substrate structures could provide a similar effect if compatible with the desired spectroscopic application.

In addition, by measuring in the time rather than frequency domain, the resonant signal can be temporally separated from the nonresonant both near- and far-field background signal contributions for pump pulse durations shorter than the molecular dephasing time. Especially if the target resonances have narrow line widths (i.e., long FID), the main impulse peak, where all of the instantaneous nonresonant and background information is contained, need not even be acquired. Without that data, and its associated noise, greater dynamic range in the tail is possible, better signal-to-noise and sensitivity is expected, and direct spectroscopic imaging is possible.

Lastly, the acquisition of the optical signal at discrete harmonics of the cantilever oscillation has considerable drawbacks. With increasing harmonics, while the near-field signal contrast improves, the s/n decreases. Therefore replacing the discrete harmonics detection with a multiharmonics analysis of the digitized time trace could provide for a much more advanced imaging modality. With this improvement and conditions, the ultimate sensitivity goal of single molecule infrared vibrational spectroscopy should readily be attainable.

Although other surface spectroscopies such as sum frequency generation (SFG) in a spectral hole burning or photon echo implementation can separate the homogeneous and inhomogeneous ensembles, they cannot provide any insight into the underlying spatial distributions of different molecular populations. Beyond greater sensitivity, the use of a tunable ultrafast laser source opens up the possibility of doing more sophisticated near-field experiments, such as infrared near-field pump probe spectroscopy or nanoscale two-dimensional Fourier transform infrared spectroscopy.

In summary, we have demonstrated femtosecond time-domain *s*-SNOM infrared molecular nanospectroscopy of a SAM on gold with a sensitivity of <100 molecular oscillators, enabled by a high and molecular bandwidth matched spectral irradiance, and the selective time-resolved resonant near-field FID signal amplification by interferometric heterodyne detection. We have shown the range and validity of the spectral phase approximation to directly relate the *s*-SNOM spectra to the molecular absorption and line shape, free of any background interference. These results, with further technical improvements as discussed, put *s*-SNOM on track to achieve true single molecule sensitivity.

■ ASSOCIATED CONTENT

Ⓢ Supporting Information

Further technical details on the spectral phase analysis used in this paper, including derivation and limitations, is included in the Supporting Information. This material is available free of charge via the Internet at http://pubs.acs.org/.

■ AUTHOR INFORMATION

Corresponding Author

*E-mail: markus.raschke@colorado.edu.

Notes

The authors declare no competing financial interest.

■ ACKNOWLEDGMENTS

We are indebted to Steve Baldelli for help with sample material and preparation. We thank Andrew Jones and Rob Olmon for valuable discussions and support at various stages of the experiments. Funding was provided by the National Science Foundation (NSF CAREER Grant CHE 0748226) and a partner proposal by the Environmental Molecular Sciences Laboratory (EMSL), a national scientific user facility from the DOE's Office of Biological and Environmental Research at Pacific Northwest National Laboratory (PNNL). PNNL is

operated by Battelle for the U.S. DOE under the contract DEAC06-76RL01830.

REFERENCES

(1) Steidtner, J.; Pettinger, B. Tip-Enhanced Raman Spectroscopy and Microscopy on Single Dye Molecules with 15 nm Resolution. *Phys. Rev. Lett.* **2008**, *100*, 236101.
(2) Knoll, B.; Keilmann, F. Near-Field Probing of Vibrational Absorption for Chemical Microscopy. *Nature* **1999**, *399*, 134−137.
(3) Stipe, B. C.; Rezaei, M. A.; Ho, W. Single-Molecule Vibrational Spectroscopy. *Science* **1998**, *280*, 1732.
(4) Ogawa, N.; Mikaelian, G.; Ho, W. Spatial Variations in Submolecular Vibronic Spectroscopy on a Thin Insulating Film. *Phys. Rev. Lett.* **2007**, *98*, 166103.
(5) Miller, L. M.; Dumas, P. Chemical Imaging of Biological Tissue with Synchrotron Infrared Light. *Biochim. Biophys. Acta* **2006**, *1758*, 846.
(6) Garczarek, F.; Gerwert1, K. Functional Waters in Intraprotein Proton Transfer Monitored by FTIR Difference Spectroscopy. *Nature* **2006**, *439*, 109.
(7) Adler, F.; Maslowski, P.; Foltynowicz, A.; Cossel, K. C.; Briles, T. C.; Hartl, I.; Ye, J. Mid-infrared Fourier Transform Spectroscopy with a Broadband Frequency Comb. *Opt. Express* **2010**, *18*, 21861.
(8) Neacsu, C.; Dreyer, J.; Behr, N.; Raschke, M. Scanning-Probe Raman Spectroscopy with Single-Molecule Sensitivity. *Phys. Rev. B* **2006**, *73*, 193406.
(9) Zhang, W.; Yeo, B. S.; Schmid, T.; Zenobi, R. Single Molecule Tip-Enhanced Raman Spectroscopy with Silver Tips. *J. Phys. Chem. C* **2007**, *111*, 1733.
(10) Akhremitchev, B. B.; Sun, Y.; Stebounova, L.; Walker, G. C. Monolayer-Sensitive Infrared Imaging of DNA Stripes Using Apertureless Near-Field Microscopy. *Langmuir* **2002**, *18*, 5325−5328.
(11) Taubner, T.; Hillenbrand, R.; Keilmann, F. Nanoscale Polymer Recognition by Spectral Signature in Scattering Infrared Near-Field Microscopy. *Appl. Phys. Lett.* **2004**, *85*, 5064.
(12) Raschke, M. B.; Molina, L.; Elsaesser, T.; Kim, D. H.; Knoll, W.; Hinrichs, K. Apertureless Near-Field Vibrational Imaging of Block-Copolymer Nanostructures with Ultrahigh Spatial Resolution. *ChemPhysChem* **2005**, *6*, 2197.
(13) Kopf, I.; Samson, J.-S.; Wollny, G.; Grunwald, C.; Bründermann, E.; Havenith, M. Chemical Imaging of Microstructured Self-Assembled Monolayers with Nanometer Resolution. *J. Phys. Chem. C* **2007**, *111*, 8166−8171.
(14) Amarie, S.; Ganz, T.; Keilmann, F. Mid-infrared Near-Field Spectroscopy. *Opt. Express* **2009**, *17*, 21794−21801.
(15) Amarie, S.; Zaslansky, P.; Kajihara, Y.; Griesshaber, E.; Schmahl, W. W.; Keilmann, F. Nano-FTIR Chemical Mapping of Minerals in Biological Materials. *Beilstein J. Nanotechnol.* **2012**, *3*, 312−323.
(16) In order to quantitatively compare IR absorption and Raman scattering cross sections, assuming a high collection efficiency of Raman light with NA = 0.8, corresponding to a solid angle of $\Theta = 0.8\pi$, $\sigma^{\mathrm{Raman}} \times \Theta = 2.5 \times 10^{-31}$ cm^2/molecule.
(17) Ocelic, N.; Huber, A.; Hillenbrand, R. Pseudoheterodyne Detection for Background-Free Near-Field Spectroscopy. *Appl. Phys. Lett.* **2006**, *89*, 101124.
(18) Huth, F.; Schnell, M.; Wittborn, J.; Ocelic, N.; Hillenbrand, R. Infrared-Spectroscopic Nanoimaging with a Thermal Source. *Nat. Mater.* **2011**, *10*, 352−356.
(19) Everall, N., Griffiths, P., Chalmers, J. M., Eds. *Vibrational Spectroscopy of Polymers: Principles and Practice*; Wiley: New York, 2007.
(20) Cvitkovic, A.; Ocelic, N.; Hillenbrand, R. Analytical Model for Quantitative Prediction of Material Contrasts in Scattering-Type Near-Field Optical Microscopy. *Opt. Express* **2007**, *15*, 8550.
(21) Deutsch, B.; Hillenbrand, R.; Novotny, L. Near-Field Amplitude and Phase Recovery Using Phase-Shifting Interferometry. *Opt. Express* **2008**, *16*, 494.
(22) Stiegler, J. M.; Abate, Y.; Cvitkovic, A.; Romanyuk, Y. E.; Huber, A. J.; Leone, S. R.; Hillenbrand, R. Nanoscale Infrared Absorption Spectroscopy of Individual Nanoparticles Enabled by Scattering-Type Near-Field Microscopy. *ACS Nano* **2011**, *5*, 6494.
(23) Zhang, L. M.; Andreev, G. O.; Fei, Z.; McLeod, A. S.; Dominguez, G.; Thiemens, M.; Castro-Neto, A. H.; Basov, D. N.; Fogler, M. M. Near-Field Spectroscopy of Silicon Dioxide Thin Films. *Phys. Rev. B* **2012**, *85*, 075419.
(24) The *s*-SNOM FID signal is a predominantly radiative vibrational resonant near-field signal. Decay of the far-field vibrational IR polarization is almost exclusively nonradiative due to the efficient intra- and intermolecular coupling in the molecular condensed phase. With increasing tip−sample coupling, an intrinsic decrease in decoherence rate is expected and can give rise to an apparent increase in *s*-SNOM line width.[36]
(25) Brehm, M.; Taubner, T.; Hillenbrand, R.; Keilmann, F. Infrared Spectroscopic Mapping of Single Nanoparticles and Viruses at Nanoscale Resolution. *Nano Lett.* **2006**, *6*, 1307−1310.
(26) Aizpurua, J.; Taubner, T.; de Abajo, F. J. G.; Brehm, M.; Hillenbrand, R. Substrate-enhanced Infrared Near-field Spectroscopy. *Opt. Express* **2008**, *16*, 1529.
(27) Ehret, S.; Schneider, H. Generation of Subpicosecond Infrared Pulses Tunable Between 5.2 μm and 18 μm at a Repetition Rate of 76 MHz. *Appl. Phys. B: Lasers Opt.* **1998**, *66*, 27−30.
(28) Ulman, A. Formation and Structure of Self-Assembled Monolayers. *Chem. Rev.* **1996**, *96*, 1533.
(29) Arnold, R.; Azzam, W.; Terfort, A.; Wöll, C. Preparation, Modification, and Crystallinity of Aliphatic and Aromatic Carboxylic Acid Terminated Self-Assembled Monolayers. *Langmuir* **2002**, *18*, 3980.
(30) Schreiber, F. Self-Assembled Monolayers: From 'Simple' Model Systems to Biofunctionalized Interfaces. *J. Phys.: Condens. Matter* **2004**, *16*, R881.
(31) Raschke, M. B.; Lienau, C. Apertureless Near-Field Optical Microscopy: Tip−Sample Coupling in Elastic Light Scattering. *Appl. Phys. Lett.* **2003**, *83*, 5089−5091.
(32) Lang, W. C.; Forinash, K. Time-Frequency Analysis with the Continuous Wavelet Transform. *Am. J. Phys.* **1998**, *66*, 794.
(33) Anderson, A.; Deryckx, K. S.; Xu, X. G.; Steinmeyer, G.; Raschke, M. B. Few-Femtosecond Plasmon Dephasing of a Single Metallic Nanostructure from Optical Response Function Reconstruction by Interferometric Frequency Resolved Optical Gating. *Nano Lett.* **2010**, *10*, 2519−2524.
(34) Xu, X. G.; Konorov, S. O.; Hepburn, J. W.; Milner, V. Background-Free Coherent Raman Spectroscopy by Detecting the Spectral Phase of Molecular Vibrations. *Opt. Lett.* **2008**, *33*, 1177.
(35) Marchev, G.; Tyazhev, A.; Vedenyapin, V.; Kolker, D.; Yelisseyev, A.; Lobanov, S.; Isaenko, L.; Zondy, J. J.; Petrov, V. Nd:YAG Pumped Nanosecond Optical Parametric Oscillator Based on $LiInSe_2$ With Tunability Extending From 4.7 to 8.7 Micron. *Opt. Express* **2009**, *17*, 13441−13446.
(36) Xu, X.; Raschke, M. Ultrafast Coherent Vibrational Dynamics and Control on the Nanoscale. Manuscript in preparation, 2012.

NOTE ADDED IN PROOF

After acceptance of this manuscript, we became aware of a related work demonstrating molecular *s*-SNOM vibrational spectroscopy following a similar approach by Huth et al. (Huth, F.; Govyadinov, A.; Amarie, S.; Nuansing, W.; Keilmann, F.; Hillenbrand, R. Nano-FTIR Absorption Spectroscopy of Molecular Fingerprints at 20 nm Spatial Resolution, *Nano Lett.* **2012**, in press, DOI: 10.1021/nl301159v).